MDPI

Article

Statistical Study of Geo-Effectiveness of Planar Magnetic Structures Evolved within ICME's

Kalpesh Ghag [1], Bhagyashri Sathe [1], Anil Raghav [1,*], Zubair Shaikh [2], Digvijay Mishra [1], Ankush Bhaskar [3], Tarun Kumar Pant [3], Omkar Dhamane [1], Prathmesh Tari [1], Prachi Pathare [1], Vinit Pawaskar [1], Kishor Kumbhar [1] and Greg Hilbert [1]

[1] Department of Physics, University of Mumbai, Vidyanagari, Santacruz (E), Mumbai 400098, India
[2] Space Sciences Laboratory, University of California, Berkeley, CA 94720, USA
[3] Space Physics Laboratory, Vikram Sarabhai Space Centre, ISRO, Thiruvananthapuram 695022, India
[*] Correspondence: anil.raghav@physics.mu.ac.in

Abstract: Interplanetary coronal mass ejections (ICME) are large-scale eruptions from the Sun and prominent drivers of space weather disturbances, especially intense/extreme geomagnetic storms. Recent studies by our group showed that ICME sheaths and/or magnetic clouds (MC) could be transformed into a planar magnetic structure (PMS) and speculate that these structures might be more geo-effective. Thus, we statistically investigated the geo-effectiveness of planar and non-planar ICME sheaths and MC regions. We analyzed 420 ICME events observed from 1998 to 2017, and we found that the number of intense (-100 to -200 nT) and extreme (<-200 nT) geomagnetic storms are large during planar ICMEs (almost double) compared to non-planar ICMEs. In fact, almost all the extreme storm events occur during PMS molded ICME crossover. The observations suggest that planar structures are more geo-effective than non-planar structures. Thus, the current study helps us to understand the energy transfer mechanism from the ICME/solar wind into the magnetosphere, and space-weather events.

Keywords: geomagnetic storm; interplanetary coronal mass ejection; planar magnetic structure

1. Introduction

Since the last century, researchers have been aware of the Earth's magnetic cavity called the magnetosphere, which was continuously shielding us from highly energetic cosmic ray radiation and solar transient events. The Carrington event in September 1859 was an eye-opening scenario for the world. It has been discussed in many news articles that the telegraph workers during that time received an electric shock after touching the telegraph instruments, and the telegraph papers were burned. This raises the question of what would be the scenario if such severe events occurred in the current satellite era. The geomagnetic storm is the root cause of this global threat. It is a temporary disturbance to the Earth's magnetosphere, where the horizontal component of the Earth's magnetic field decreases for 12 to 24 h (Gonzalez et al. [1], Akasofu [2]). This may affect electrical power grids, cause the erosion of oil and gas pipelines, affect GPS navigation and high-frequency radio communications, cause ionosphere changes, affect radiation belt dynamics, cause damage to satellite electronics and solar panels, and cause satellite drag (Marusek [3], Boerner et al. [4], Baker et al. [5], Ferguson et al. [6], Oliveira et al. [7], Boteler [8]). Thus, in the current satellite era, the study of a geomagnetic storm has both scientific and technological importance and significance to the global economy.

Reported studies over the decades clearly understand the geomagnetic storm's profile. At the initial phase, a sudden increase in the geomagnetic field is observed. This is known as sudden storm commencement (SSC). The SSC is associated with the Chapman Ferraro current or magnetopause current (Chapman and Bartels [9]). Followed by the SSC, the decrease in the horizontal component of the magnetic field is observed, called

the main phase of the geomagnetic storm. The equatorial ring current enhancement is the primary reason behind the storm's main phase. The southward component of the interplanetary magnetic field ($-B_z$) reconnects with the north Earth's magnetic field and allows large numbers of energetic particles into Earth's magnetosphere. This causes the enhancement in ring current and the decrease in the resultant horizontal component of the geomagnetic field. During the main phase, the geomagnetic field reduces from -50 nt to -600 nT. However, during the above-mentioned Carrington superstorm, the main phase reaches a peak value of ~ -1760 nT (Tsurutani et al. [10], Hayakawa et al. [11]). The geomagnetic field starts to recover as soon as the enhanced ring current starts decaying with the help of processes such as charge exchanges, Coulomb interactions, or wave–particle interactions (Dungey [12], Choraghe et al. [13], Kozyra and Liemohn [14], Daglis et al. [15], Jordanova [16], and Chen et al. [17]). This phase is known as the recovery phase. Interplanetary coronal mass ejection (ICME) is one of the significant causes of geomagnetic storms (Akasofu [2], Richardson et al. [18], Richardson and Cane [19], Tsurutani et al. [20]). ICME carries the solid southward magnetic field component, which reconnects with the northward Earth's magnetic field, deposits large amounts of energy, and charged particles in Earth's magnetosphere (Gonzalez et al. [1], Dungey [12], O'Brien and McPherron [21]). The in situ observations of the ICME depict three notable structures, i.e., forward propagating shock, the compressed and turbulent sheath region, and the orderly magnetized flux rope connected to the Sun (Burlaga [22], Bothmer and Schwenn [23], Kilpua et al. [24], Zurbuchen and Richardson [25]). The reported studies suggest that the nature of the geomagnetic storms caused by a sheath and magnetic cloud has different impacts on magneto-tail, auroral activity, magnetosphere asymmetry, etc. (See Tsurutani et al. [26], Schwenn et al. [27], Koskinen and Huttunen [28], and Huttunen et al. [29] and the reference therein).

During periods of solar minimum, the interplanetary medium experiences heightened activity primarily driven by high-speed streams (HSS) originating from coronal holes (Tsurutani et al. [30,31], Yermolaev et al. [32]). These HSS encounter slower solar wind, giving rise to the formation of stream interaction regions (SIRs) (Burlaga and Lepping [33]). Moreover, SIRs, or their evolved forms such as corotating interaction regions (CIRs), play a significant role in the occurrence of geomagnetic storms. The B_z component of the magnetic field within SIRs/CIRs exhibits notable fluctuations, resulting in irregular and relatively weaker main phases of magnetic storms. Furthermore, the heliocentric current sheet (HCS) structure in the solar wind also plays a role in the occurrence of geomagnetic storms. The high-density plasma within the HCS can contribute to the "initial phase" of a geomagnetic storm (Gonzalez et al. [34]). It is crucial to emphasize that the profile of a storm resulting from solar wind structures is distinctly different from that caused by ICMEs.

The near-earth plasma conditions and IMF orientation significantly influence the geomagnetic activity. Due to various interactions amongst interplanetary plasma structures and solar wind, the IMF vectors are restricted in a quasi-two-dimensional space and appear as a sheet with magnetic vectors that are parallel but orientated differently for a short period. These structures in interplanetary space are called planar magnetic structures (PMS) (Nakagawa et al. [35]). The existence of PMS in the solar wind , CIR, and ICME sheath region were reported earlier. Two physical explanations for the origin of PMS in the ICME sheath region were put forth, including (i) the parallel alignment of pre-existing microstructures and discontinuities in the solar wind and (ii) the wrapping of interplanetary magnetic field lines around the ejecta/MC (Nakagawa [36], Neugebauer et al. [37], Shaikh et al. [38]). Moreover, PMSs are also observed in the magnetic cloud region. Raghav and Shaikh [39] suggested that ICME MC can occasionally get so flattened that it shows PMS characteristics. They also suggested that this PMS-molded ICME MC cross-section can have a "pancaking" effect. It suggests that compression plays a crucial role in transforming MCs into the quasi-2D PMS structure.

Recently, it has been shown that the ICME sheath (Shaikh et al. [38], Palmerio et al. [40]) and MC (Raghav and Shaikh [39], Shaikh and Raghav [41], Raghav et al. [42]) can transform into planar magnetic structures (PMS). Shaikh et al. [38] suggest that out of 420 ICME

events, 147 (∼35%) ICME-driven sheaths are planar, whereas the remaining 273 (∼65%) are non-planar. On the other hand, Shaikh and Raghav [41] suggest that ∼121 (29%) ICME MCs are planar, whereas 299 (∼71%) are non-planar. PMSs are plane/sheet-like 2D magnetic structures in the solar wind where magnetic vectors are parallel but oriented differently for a short period within the sheet (Nakagawa et al. [35], Nakagawa [36], Neugebauer et al. [37]). They suggest that compression could be important in transforming a region into the PMS structure. They proposed that plasma properties and southward/northward oriented magnetic fields are significantly stronger than non-PMS ICME sheath/MC (Shaikh et al. [38] and Shaikh and Raghav [41]). This implies that PMS-transformed structures are more favorable for severe geomagnetic storms (McComas et al. [43,44]). Kataoka et al. [45] studied the cause of the extreme magnetic storm that occurred on March 2015 and found that the PMSs are formed downstream of ICME shock due to its less adiabatic expansion. This results in enhancing the magnetic field strength and the plasma properties responsible for a geomagnetic storm. Recent observations by Choraghe et al. [46] have identified the presence of PMSs in the vicinity of the SIR/CIR region and highlighted their contribution to intense storms induced by CIRs. In addition, (Raghav et al. [42]) also proved that the PMS transformation of ICME due to pancaking was the major cause of the Halloween superstorm that occurred on 20 November 2003. However, detailed statistical corroborations of these case studies are still unavailable. Here, we statistically investigate the role of PMS-transformed ICME substructures in terms of their geo-effectiveness.

2. Data and Results

In the present study, we selected 420 ICME events from 1998 to 2017 from the Richardson–Cane catalog available at ACE ICME catalogue https://izw1.caltech.edu/ACE/ASC/DATA/level3/icmetable2.htm (accessed on 10 September 2022). The event list is from 1998 to 2017, i.e., solar cycles 23 and 24. A similar ICME catalogue has been utilized by Shaikh et al. [38] and Shaikh and Raghav [41] to investigate the plasma characteristics of PMS-transformed ICME. In this context, the term "planar" refers to the region that has undergone PMS transformation. Shaikh et al. [38] and Shaikh and Raghav [41] classified the ICME's into the following categories:

1. Planar Sheaths: only sheaths transformed into PMS;
2. Planar MCs: only MC transformed into PMS;
3. Planar ICMEs: both sheath and MC transformed into PMS;
4. Non-planar ICMEs: neither sheaths nor MCs transformed into PMS.

Figure 1 shows the Venn diagram corresponding to the categorization of ICME events. We selected a total of 420 events, out of which 206 ICMEs are non-planar (shown with yellow shade in Figure 1). We analyzed 67 planar cloud events and 93 planar sheaths (shown by green and gray shades, respectively). We analyzed a total of 54 events, which show planarity in the sheath and magnetic cloud (dark green shaded region). We used the geomagnetic storm index, e.g., disturbances storm time index (Dst) and the Sym-H index from the OMNI database (available at http://omniweb.gsfc.nasa.gov/form/dxl.html (accessed on 10 September 2022)) to study magnetospheric disturbed conditions (Bergin et al. [47]). We categorized geomagnetic storms according to their intensity, viz. extreme geomagnetic storms (<-200 nT), intense geomagnetic storms (-100 nT to -200 nT), moderate geomagnetic storms (-50 nT to -100 nT), and weak geomagnetic storms (>-50 nT). The minimum and maximum SYM-H values for each distinct region are identified as explained in Figure 2. We calculated the mean SYM-H value for each distribution. The standard error is calculated as per the method mentioned in Yermolaev et al. [48]. Kindly note that the maximum SYM-H observation within the ICME MC is not useful since it does not actually contribute to the initial phase.
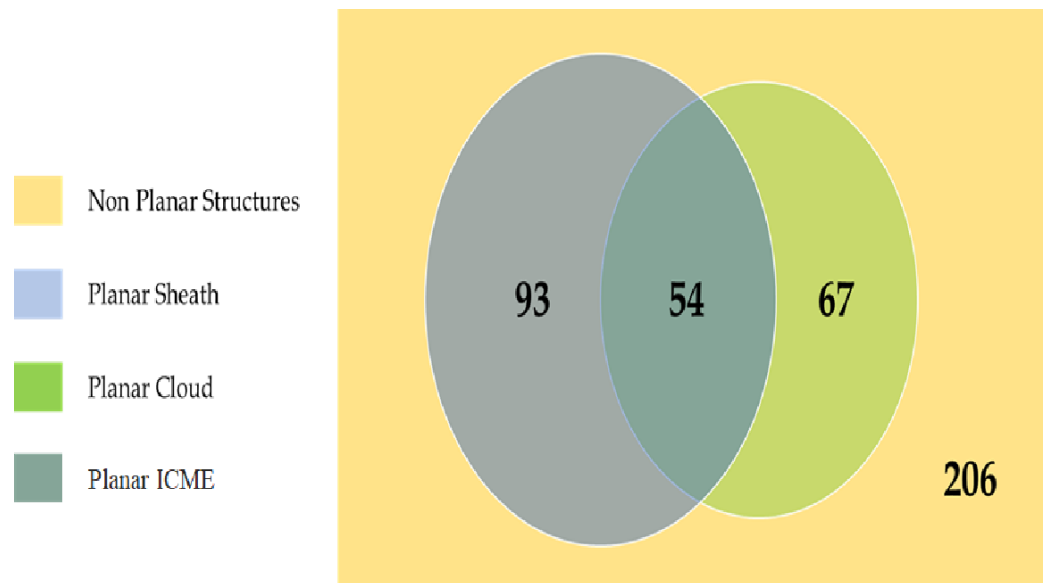
Figure 1. A Venn diagram showing different groups of ICMEs classified by Shaikh et al. [38] and Shaikh and Raghav [41].
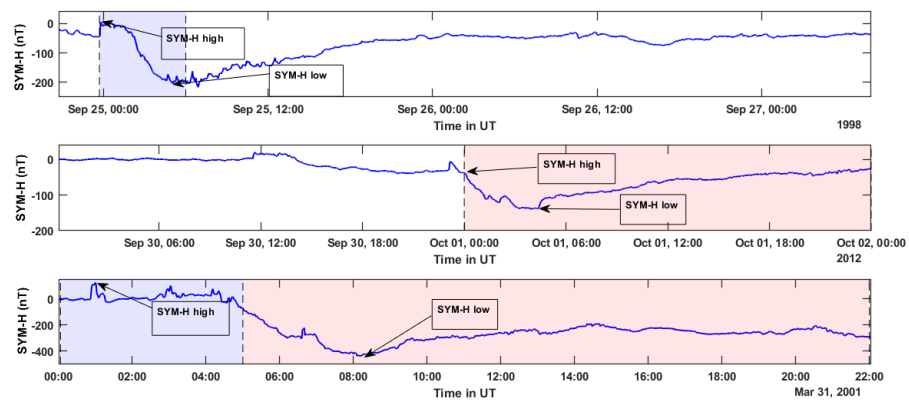
Figure 2. Representation of the selection criteria for SYM-H index for the events: the uppermost panel shows PMS in the sheath, the middle panel shows PMS in the cloud, and the bottom panel shows PMS in both sheath and cloud. The sheath is indicated by blue-shaded region, and a magnetic cloud is shown by the red-shaded region.

Shaikh et al. [38] and Shaikh and Raghav [49] suggest that out of 420 ICME events, 121 (29%) ICME MCs transformed into PMS, 147 (35%) ICME sheaths transformed into PMS, and 54 ICMEs (both sheath and MC) transformed into PMS, whereas the remaining 206 (49%) ICMEs sheath and MCs events did not have any PMS signature (See Figure 1). Further, we studied the main phase minimum and initial phase maximum values of the SYM-H index during each such passage. Figure 3 illustrates the distribution of SYM-H high and SYM-H low. In the left column, the distributions of the maximum initial phase (SYM-H high) are shown for (a) non-planar ICMEs, (c) planar magnetic clouds, (e) planar sheaths, and (g) planar ICMEs. On the right column, the distributions of the minimum main phase (SYM-H low) are displayed for (b) non-planar ICMEs, (d) planar magnetic clouds, (f) planar sheaths, and (h) planar ICMEs.

For the main phase (right column of Figure 3), the top panel (b) shows distribution during the non-planar ICMEs. The distribution has asymmetrical tail toward lower SYM-H index values, where the mean is about -57 ± 3 nT. Panel (d) also shows similar distribution like non-planar ICMEs during the planar MCs, and the mean is about -71 ± 4 nT. Similarly, we noted that the distribution has an asymmetrical tail toward lower SYM-H index values during planar sheaths and planar ICMEs also. During the planar sheaths

(panel (f); the mean is about -58 ± 4 nT, whereas during planar ICMEs (panel (h)), the mean values is -98 ± 7 nT. Thus, we observed a stronger depression of SYM-H during the PMS-transformed structure, which suggests PMS is more favourable for enhancing geo-effectiveness.
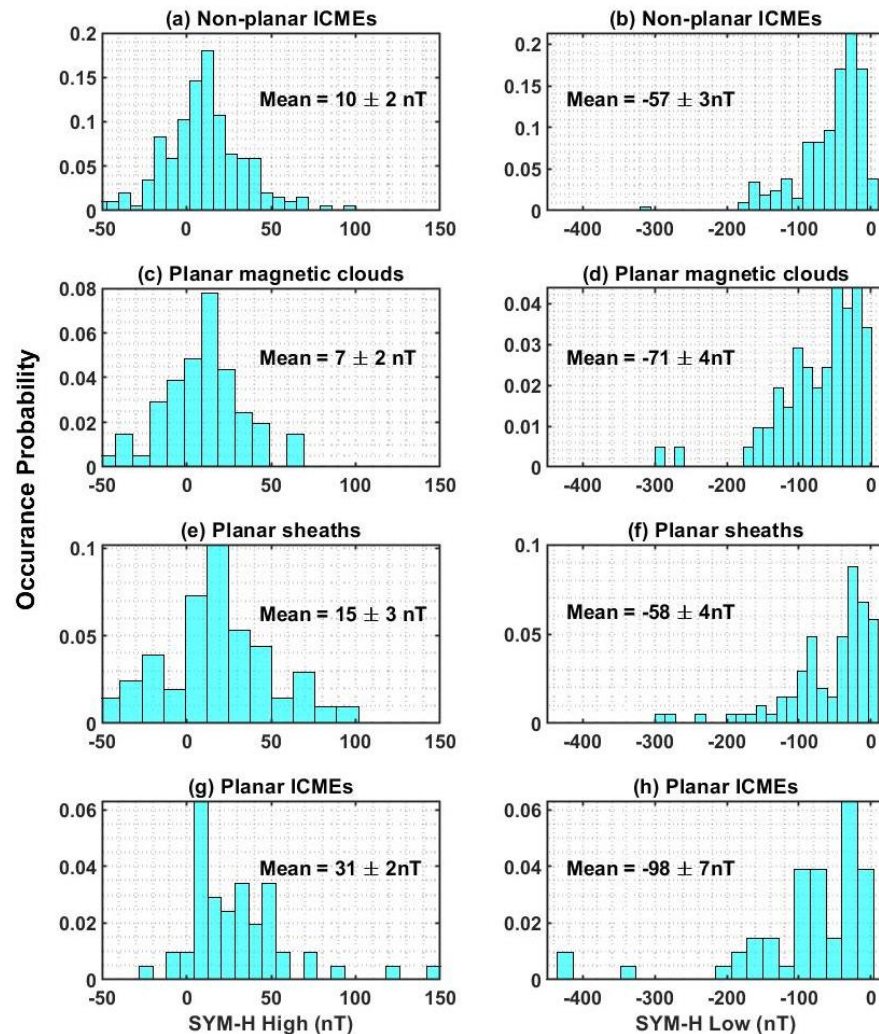
Figure 3. The left column indicates the distribution of initial phase maximum (SYM-H high) for (**a**) non-planar ICMEs, (**c**) planar magnetic clouds, (**e**) planar sheaths, and (**g**) planar ICMEs. The right column shows the distribution of main phase minimum (SYM-H low) for (**b**) non-planar ICMEs, (**d**) planar magnetic clouds, (**f**) planar sheaths, and (**h**) planar ICMEs.

Similarly, Figure 3 (left column) illustrates the distribution of the initial phase maximum (SYM-H high) during the above different categories. During non-planar ICMEs (panel (a)), we observed the normal distribution of SYM-H with a mean value of 10.0 ± 2 nT. Similarly, in the case of planar sheaths (panel (e)) and planer MCs (panel (c)), the distributions are close to the normal distribution. The mean value during the planar sheaths is 15 ± 2 nT, whereas, during planar MCs, the mean is 7 ± 2 nT. Moreover, during planar ICMEs (panel (g)), the distribution has an asymmetrical tail toward higher SYM-H index values, and the mean value is 31 ± 2 nT. It is important to note that, during planar ICMEs, we observe a significant enhancement in the value of SYM-H compared to non-planar ICMEs. In fact, we observed a couple of cases with an amplitude higher than 100 nT during the initial phase of completely transformed ICMEs. Thus, it is clear that PMS-transformed structures significantly enhance the geomagnetic storm's initial phase. We noticed that both planar and non-planar ICME events displayed almost symmetrical distributions of high

SYM-H values. However, when it came to low SYM-H values, the distributions showed asymmetry towards lower SYM-H values. This asymmetry can be attributed to the fact that the right side of the SYM-H low distribution comprises storms with positive amplitudes. It is crucial to emphasize that low SYM-H values cannot be positive unless there is an extremely weak storm present, where the minimum SYM-H value is greater than 0.

In addition to this, we also noted that out of 206 non-planar ICMEs, ≈54 % resulted in weak geomagnetic storms, ≈30% related to moderate storms, ≈14% were associated with the intense geomagnetic storms, and only ≈0.5% contributed to extreme geomagnetic storms. In contrast, we observed significantly more extreme storms compared to non-planar ICMEs, i.e., planar sheaths comprised ≈5%, planar MCs comprised ≈3%, and planar ICMEs comprised ≈9% extreme geomagnetic storms (see Table 1 for more detail). Thus, it also supports the hypothesis that the occurrence of extreme geomagnetic storm events during planar ICMEs, planar sheath, and planar clouds is high.

Table 1. Contribution of PMS into different categories of geomagnetic storms.

Groups	Weak (>−50 nT)	Moderate (−50 nT to −100 nT)	Intense (−100 nT to −200 nT)	Extreme (>−200 nT)
Planar ICMEs	38.88%	25.92%	25.92%	9.25%
Planar MCs	43.28%	31.34%	22.38%	2.98%
Planar sheaths	58.06%	22.58%	13.97%	5.37%
Non-Planar ICMEs	54.85%	30.58%	14.07%	0.48%

It is important to note that magnetic cloud (MC) structures are not present in all ICMEs. This means some ICMEs may not exhibit all the expected characteristics of MCs, but they may still display certain indicators. These ICMEs typically lack the usual attributes associated with MCs, such as a smooth rotation of the IMF and an enhanced magnetic field. Consequently, when ICMEs do not encompass all the defining features of an MC, they are termed non-magnetic clouds (NMC) or ejecta. The ACE-ICME catalog available online, compiled by Richardson and Cane, has classified ICMEs based on their magnetic cloud (MC) and ejecta structures. Upon analyzing 206 ICMEs with nonplanar trajectories, we observed that 45 of them (21.53%) exhibited signatures of proper MCs, while 167 (78.15%) displayed features of ejecta (See Table 2 for details). Furthermore, among the 67 ICMEs with planar magnetic cloud events in our earlier part of the study, 36 (53.73%) demonstrated standard MC features, whereas 31 (46.26%) exhibited characteristics of ejecta. For our analysis, both categories were considered as "magnetic clouds." Examining the 93 sheath events, we found that 60 of them (64.51%) occurred in front of magnetic clouds, while 33 (35.48%) were positioned ahead of non-magnetic clouds. Additionally, out of the total ICMEs evaluated, 25 (46.29%) were completely planar, encompassing both the sheath and MC components, while 29 (53.70%) ICMEs were entirely planar but displayed ejecta characteristics. Out of 161 ejecta events, only one extreme geomagnetic storm was caused by a non-planar ejecta (See Table 3 for details). However, among the 45 non-planar magnetic clouds, there were no extreme geomagnetic storms. Conversely, there was one extreme geomagnetic storm event attributed to a planar magnetic cloud but no extreme storms caused by planar ejecta. Out of the 60 planar sheaths preceding the ejecta, 4 of them resulted in extreme geomagnetic storms. Additionally, out of the 33 events involving a planar sheath ahead of a magnetic cloud, 8 extreme geomagnetic storms occurred. In the case of planar ICMEs, there were 2 extreme storm events out of 25 events with ejecta, and there were 3 extreme storm events out of 29 magnetic clouds. Overall, the highest percentage of extreme storms was found in planar sheath events that preceded the magnetic cloud.

Table 2. Categorisation of ICME events into magnetic clouds and non-magnetic clouds.

Categories	Magnetic Cloud	Ejecta
Non-planar structures	21.53%	78.15%
Planar magnetic clouds	53.73%	46.26%
Planar sheaths	64.51%	35.48%
Planar ICME	46.29%	53.70%

3. Discussion

The most important factors for a geomagnetic storm are large and long-duration interplanetary B_z and dusk-ward (E_y) convection electric field (see, e.g., Kamide et al. [50], Gonzalez et al. [1], Aguado et al. [51], Gonzalez et al. [34], Akasofu [2], and references therein). These studies propose that the primary mechanism for energy transport from interplanetary space to the Earth's magnetosphere is the coupling resulting from magnetic reconnection between the southward-directed interplanetary magnetic field (IMF) component (B_z) and the Earth's magnetic field. Besides this, some other factors can contribute to the profile of geomagnetic storms, viz. solar wind density (N_p), solar wind velocity (V_p), and solar wind dynamic pressure (P_d) etc. The role of the solar wind density (N_p) on solar wind in geomagnetic storm is not straightforward. O'Brien and McPherron [52] provide statistical evidence suggesting that the Dst index, which represents geomagnetic activity, is not heavily dependent on the driver function that includes the solar wind density (N_p). However, some studies proposed that N_p ought to behave as a medium for the solar wind's energy transfer to the inner magnetosphere. Borovsky et al. [53] demonstrated a connection between the solar wind density (N_p) and the plasma density at geosynchronous orbit within the Earth's magnetosphere. The predictions from the inner magnetosphere simulations suggest that the ion and electron density near the geosynchronous orbit should influence ring current amplitude (Jordanova et al. [54], Liemohn et al. [55]). This suggests the indirect relationship between N_p and geomagnetic storms. Along with N_p, the solar wind speed does not have any direct correlation with geomagnetic indices. However, the solar wind dynamic pressure (the function of N_p and V_p i.e., $P_d = N_p m_p V_p^2$) is a major contributor in geomagnetic activity. Fenrich and Luhmann [56] suggests that during the passage of enhanced dynamic pressure, the ring current injection rate is found to increase. Wang et al. [57] empirically shows the dynamic pressure effect on the ring current injection using Dst index. They also suggest a low ring current decay rate in high dynamic pressure conditions.

Shaikh et al. [38] and Shaikh and Raghav [41] show that the magnitude of plasma parameters and southward/northward B_z within the planar sheaths and planar MCs is almost double with respect to non-planar ICMEs, respectively (see the summary of these results in Table 4). This is due to the compression associated with planar structures, which may cause plasma pile-up. Thus, they speculated that PMS-transformed magnetic structures are more favourable for generating great geomagnetic storms. However, the following question remains: How geoeffective are planar ICMEs?

In this paper, we use statistical analysis to investigate the geo-effectiveness of the PMS molded ICME and its sub-structures (sheath and magnetic cloud). We observed that during planar sheaths, planar MCs, and planar ICMEs, the average low SYM-H index is $\sim -58 \pm 4$ nT, $\sim -71 \pm 4$ nT, and $\sim -98 \pm 7$ nT, respectively, whereas in the case of non-planar ICMEs, the mean value of the low SYM-H index is $\sim -57 \pm 3$ nT. Furthermore, the percentage occurrence of an extreme geomagnetic storm is rare ($\approx 0.4\%$) in non-planar ICME-induced storms. However, the percentage of an extreme geomagnetic storm is increased to $\approx 5\%$ for planar sheath-induced storms. In ICMEs with both the planar sheath and magnetic cloud, the percentage of the extreme geomagnetic storm increases to $\approx 9\%$. This implies that the ICMEs with both a planar sheath and planar clouds are more geoeffective. In the case of both planar sheath and planar cloud crossover,

the magnetosphere is dually encountered by the enhanced plasma parameters and IMF strength of the planar structures. Hence, we observed a greater percentage of an extreme geomagnetic storm in this case.

Table 3. Geoeffectiveness of the planar and non-planar structures considering ejecta and magnetic cloud.

Characteristics	Non-PMS		PMS-MC		PMS-Sheath		Both PMS	
	Ejecta (161)	Cloud (45)	Ejecta (31)	Cloud (36)	Ejecta (60)	Cloud (33)	Ejecta (25)	Cloud (29)
Extreme	1	0	0	1	4	8	2	3
Intense	14	15	7	11	12	8	6	8
Moderate	46	18	8	14	26	4	5	10
Weak	110	12	16	10	18	13	12	8

We found a similar trend in intense geomagnetic storms (see Table 1 for details). Furthermore, the occurrence percentage of weak and moderate storms is much higher during the crossover of non-planar ICMEs. Thus, we conclude that PMS-transformed ICMEs and their sub-structures are more geo-effective than non-planar ICMEs. This might be due to the combined effect of all the enhanced solar wind plasma parameters and IMF that significantly affect the ring current dynamics and could be responsible for enhanced geo-effectiveness.

Table 4. Comparison of different plasma parameters in planar and non-planar ICME sheath and magnetic cloud taken from Shaikh et al. [38] and Shaikh and Raghav [41].

	ICME Sheath		ICME Magnetic Cloud	
	Non-Planar	Planar	Non-Planar	Planar
B (nT)	9.17	13.57	8.66	12.20
Bz_{min} (nT)	−6.91	−15.43	−9.46	−13.67
Bz_{max} (nT)	7.71	14.71	8.09	13.10
Np (cc^{-1})	9.66	13.41	6.22	8.40
Vp (kms^{-1})	482.79	510.80	458.95	451.79
Tp ($\times 10^5$ K)	1.37	1.97	0.52	0.51

The geoeffectiveness of the sheath has been a point of discussion for the various studies in recent years. Huttunen and Koskinen [58] studied the geomagnetic storm from 1997 to 2002 using WIND and ACE spacecraft and showed that the largest portion of intense magnetic storms was caused by post-shock streams and sheath regions of ICME. In addition, Guo et al. [59] suggested that during ICME-driven storms (especially magnetic cloud-driven storms), the solar wind-magnetosphere coupling functions and geomagnetic indices exhibit a slower and more gradual increase and recovery compared to sheath-driven storms. In contrast, sheath-driven storms tend to have larger peak values in these parameters. This suggests that the dynamics and impact of ICME-driven storms differ from those driven by sheaths, with the former displaying a more prolonged and less intense response in the solar wind-magnetosphere system. Later, Yermolaev et al. [60] proposed that the sheath has a higher occurrence rate and efficiency of geomagnetic storms. We also observed a higher frequency of extreme storms during the crossover of planar sheaths (approximately 5%) compared to planar MC passages (around 2.98%). However, we noted a higher occurrence of intense storms associated with planar MCs (approximately 22%) than planar sheaths (approximately 14%). Hence, we conclude that planar MCs are more likely to result in intense storms, while planar sheaths contribute to the occurrence of

extreme geoeffective events. It is indeed fascinating to investigate the degree to which planarity amplifies the geoeffectiveness of sheaths, considering that sheaths are already acknowledged as impacting Earth's geomagnetic activity. Therefore, we intend to conduct a thorough investigation of this matter in the future.

Moreover, we also observed a high SYM-H index during the passage of planar sheath, planar MCs, and planar ICMEs compared to the non-planar ICMEs. The mean of high SYM-H value (in the initial phase of the storm) during planar ICMEs is 31 nT, and this is three times more than the high SYM-H value found in non-planar ICMEs (10 nT). This indicates that planar structures are also significantly contributing to the initial phase of the storm. But how could this happen? Generally, we observe the storm's initial phase due to an increase in magnetopause current (Akasofu [2]). This means that the magnetic field generated due to this current increases the geomagnetic field. When solar wind compresses the magnetosphere, it moves the regions toward the Earth, which results in the enhancement of magnetopause current. Due to the predominantly northward orientation of the magnetic field within the region, the current will flow from the dawn to dusk direction along the equatorial magnetopause and from the dusk to dawn direction along the high-latitude magnetopause, specifically tail-ward of the cusp openings. For the studied events, we know that compression is the main factor that converts a region to a quasi-planar structure (Nakagawa et al. [35], Palmerio et al. [40]). So, high density and enhanced northward interplanetary magnetic field within the planar structures causes high compression of the magnetosphere compared to non-planar structures. Thus, it causes the development of intense magnetopause currents, and we observe a high initial phase during planar structures compared to non-planar structures.

4. Conclusions

- Our study statistically confirms the hypothesis that ICMEs that are transformed into PMS are more geoeffective than non-planar ICMEs.
- The combined enhancement in the magnetic field components and plasma parameters is found in the planar sheath and MCs.
- The enhancement in the magnetopause current and ring current due to enhanced plasma conditions could be the main reason for the high geoeffectiveness of planar ICMEs.
- A detailed study may be required in this direction to find the extent of the effects of planar ICMEs on the magnetosphere, the ionosphere, the coupling between the magnetosphere and the ionosphere, etc. Our future studies will explore this direction.

References

1. Gonzalez, W.; Joselyn, J.; Kamide, Y.; Kroehl, H.; Rostoker, G.; Tsurutani, B.; Vasyliunas, V. What is a geomagnetic storm? *J. Geophys. Res.* **1994**, *99*, 5771–5792. [CrossRef]
2. Akasofu, S.I. A Review of the Current Understanding in the Study of Geomagnetic Storms. *Int. J. Earth Sci. Geophys.* **2018**, *4*, 018.
3. Marusek, J.A. *Solar Storm Threat Analysis*; Marusek, J., Ed.; Impact: Bloomfield, IN, USA, 2007.
4. Boerner, W.M.; Cole, J.B.; Goddard, W.R.; Tarnawecky, M.Z.; Shafai, L.; Hall, D.H. Impacts of solar and auroral storms on power line systems. *Space Sci. Rev.* **1983**, *35*, 195–205. [CrossRef]
5. Baker, D.; Erickson, P.; Fennell, J.; Foster, J.; Jaynes, A.; Verronen, P. Space weather effects in the Earth's radiation belts. *Space Sci. Rev.* **2018**, *214*, 1–60. [CrossRef]
6. Ferguson, D.C.; Worden, S.P.; Hastings, D.E. The space weather threat to situational awareness, communications, and positioning systems. *IEEE Trans. Plasma Sci.* **2015**, *43*, 3086–3098. [CrossRef]
7. Oliveira, D.M.; Zesta, E.; Hayakawa, H.; Bhaskar, A. Estimating satellite orbital drag during historical magnetic superstorms. *Space Weather* **2020**, *18*, e2020SW002472. [CrossRef]
8. Boteler, D. Geomagnetic hazards to conducting networks. *Nat. Hazards* **2003**, *28*, 537–561. [CrossRef]
9. Chapman, S.; Bartels, J. *Geomagnetism*; Clarendon Press: Oxford, UK, 1940; Volume 2.
10. Tsurutani, B.; Gonzalez, W.; Lakhina, G.; Alex, S. The extreme magnetic storm of 1–2 September 1859. *J. Geophys. Res.* **2003**, *108*, 2999–3002. [CrossRef]
11. Hayakawa, H.; Nevanlinna, H.; Blake, S.P.; Ebihara, Y.; Bhaskar, A.T.; Miyoshi, Y. Temporal variations of the three geomagnetic field components at colaba observatory around the carrington storm in 1859. *Astrophys. J.* **2022**, *928*, 32. [CrossRef]
12. Dungey, J.W. Interplanetary magnetic field and the auroral zones. *Phys. Rev. Lett.* **1961**, *6*, 47. [CrossRef]
13. Choraghe, K.; Raghav, A.; Chakrabarty, D.; Kasthurirangan, S.; Bijewar, N. Properties of the recovery phase of extreme storms. *J. Geophys. Res.* **2021**, *126*, e2020JA028685. [CrossRef]
14. Kozyra, J.U.; Liemohn, M.W. Ring current energy input and decay. In *Magnetospheric Imaging—The Image Prime Mission*; Springer: Berlin/Heidelberg, Germany, 2003; pp. 105–131.
15. Daglis, I.A.; Thorne, R.M.; Baumjohann, W.; Orsini, S. The terrestrial ring current: Origin, formation, and decay. *Rev. Geophys.* **1999**, *37*, 407–438.
16. Jordanova, V.K. Ring current decay. In *Ring Current Investigations*; Elsevier: Amsterdam, The Netherlands, 2020; pp. 181–223.
17. Chen, M.W.; Schulz, M.; Lyons, L.R. Modeling of ring current formation and decay: A review. *Wash. Am. Geophys. Union Geophys. Monogr. Ser.* **1997**, *98*, 173–186.
18. Richardson, I.; Webb, D.; Zhang, J.; Berdichevsky, D.; Biesecker, D.; Kasper, J.; Kataoka, R.; Steinberg, J.; Thompson, B.; Wu, C.C.; et al. Major geomagnetic storms (Dst = −100 nT) generated by corotating interaction regions. *J. Geophys. Res.* **2006**, *111*, A07S09.
19. Richardson, I.G.; Cane, H.V. Solar wind drivers of geomagnetic storms during more than four solar cycles. *J. Space Weather. Space Clim.* **2012**, *2*, A01. [CrossRef]
20. Tsurutani, B.T.; Gonzalez, W.D.; Gonzalez, A.L.; Guarnieri, F.L.; Gopalswamy, N.; Grande, M.; Kamide, Y.; Kasahara, Y.; Lu, G.; Mann, I.; et al. Corotating solar wind streams and recurrent geomagnetic activity: A review. *J. Geophys. Res.* **2006**, *111*, A07S01.
21. O'Brien, T.P.; McPherron, R.L. An empirical phase space analysis of ring current dynamics: Solar wind control of injection and decay. *J. Geophys. Res.* **2000**, *105*, 7707–7719.
22. Burlaga, L. Magnetic clouds and force-free fields with constant alpha. *J. Geophys. Res.* **1988**, *93*, 7217–7224. [CrossRef]
23. Bothmer, V.; Schwenn, R. The structure and origin of magnetic clouds in the solar wind. In *Annales Geophysicae*; Springer: Berlin/Heidelberg, Germany, 1997; Volume 16, pp. 1–24.
24. Kilpua, E.; Jian, L.; Li, Y.; Luhmann, J.; Russell, C. Observations of ICMEs and ICME-like solar wind structures from 2007–2010 using near-Earth and STEREO observations. *Sol. Phys.* **2012**, *281*, 391–409.
25. Zurbuchen, T.H.; Richardson, I.G. in situ solar wind and magnetic field signatures of interplanetary coronal mass ejections. In *Coronal Mass Ejections*; Springer: New York, NY, USA, 2006; pp. 31–43.
26. Tsurutani, B.; Lakhina, G.; Verkhoglyadova, O.P.; Gonzalez, W.; Echer, E.; Guarnieri, F. A review of interplanetary discontinuities and their geomagnetic effects. *J. Atmos. Sol. Terr. Phys.* **2011**, *73*, 5–19. [CrossRef]
27. Schwenn, R.; Dal Lago, A.; Huttunen, E.; Gonzalez, W.D. The association of coronal mass ejections with their effects near the Earth. In *Annales Geophysicae*; Copernicus GmbH: Göttingen, Germany, 2005; Volume 23, pp. 1033–1059.
28. Koskinen, H.; Huttunen, K. Geoeffectivity of coronal mass ejections. *Space Sci. Rev.* **2006**, *124*, 169–181. [CrossRef]
29. Huttunen, K.; Koskinen, H.; Karinen, A.; Mursula, K. Asymmetric development of magnetospheric storms during magnetic clouds and sheath regions. *Geophys. Res. Lett.* **2006**, *33*, L06107. [CrossRef]
30. Tsurutani, B.T.; Gonzalez, W.D.; Gonzalez, A.L.; Tang, F.; Arballo, J.K.; Okada, M. Interplanetary origin of geomagnetic activity in the declining phase of the solar cycle. *J. Geophys. Res.* **1995**, *100*, 21717–21733. [CrossRef]
31. Tsurutani, B.T.; Ho, C.M.; Arballo, J.K.; Goldstein, B.E.; Balogh, A. Large amplitude IMF fluctuations in corotating interaction regions: Ulysses at midlatitudes. *Geophys. Res. Lett.* **1995**, *22*, 3397–3400.
32. Yermolaev, Y.I.; Lodkina, I.G.; Dremukhina, L.A.; Yermolaev, M.Y.; Khokhlachev, A.A. What solar–terrestrial link researchers should know about interplanetary drivers. *Universe* **2021**, *7*, 138. [CrossRef]
33. Burlaga, L.; Lepping, R. The causes of recurrent geomagnetic storms. *Planet. Space Sci.* **1977**, *25*, 1151–1160. [CrossRef]

34. Gonzalez, W.D.; Tsurutani, B.T.; Clúa de Gonzalez, A.L. Interplanetary origin of geomagnetic storms. *Space Sci. Rev.* **1999**, *88*, 529–562. [CrossRef]

35. Nakagawa, T.; Nishida, A.; Saito, T. Planar magnetic structures in the solar wind. *Geophys. Res. Lett.* **1989**, *94*, 11761–11775. [CrossRef]

36. Nakagawa, T. Solar source of the interplanetary planar magnetic structures. *Sol. Phys.* **1993**, *147*, 169–197. [CrossRef]

37. Neugebauer, M.; Clay, D.; Gosling, J. The origins of planar magnetic structures in the solar wind. *J. Geophys. Res.* **1993**, *98*, 9383–9389. [CrossRef]

38. Shaikh, Z.I.; Raghav, A.N.; Vichare, G.; Bhaskar, A.; Mishra, W. Comparative statistical study of characteristics of plasma in planar and non-planar ICME sheaths during solar cycles 23 and 24. *Mon. Not. R. Astron. Soc.* **2020**, *494*, 2498–2508. [CrossRef]

39. Raghav, A.N.; Shaikh, Z.I. The pancaking of coronal mass ejections: An in situ attestation. *Mon. Not. R. Astron. Soc.* **2020**, *493*, L16–L21. [CrossRef]

40. Palmerio, E.; Kilpua, E.K.; Savani, N.P. Planar magnetic structures in coronal mass ejection-driven sheath regions. In *Annales Geophysicae*; Copernicus GmbH: Göttingen, Germany, 2016; Volume 34, pp. 313–322.

41. Shaikh, Z.I.; Raghav, A.N. Statistical Plasma Properties of the Planar and Nonplanar ICME Magnetic Clouds during Solar Cycles 23 and 24. *Astrophys. J.* **2022**, *938*, 146. [CrossRef]

42. Raghav, A.; Shaikh, Z.; Vemareddy, P.; Bhaskar, A.; Dhamane, O.; Ghag, K.; Tari, P.; Dayanandan, B.; Mohammed Al Suti, B. The Possible Cause of Most Intense Geomagnetic Superstorm of the 21st Century on 20 November 2003. *Sol. Phys.* **2023**, *298*, 64. [CrossRef]

43. McComas, D.; Gosling, J.; Winterhalter, D.; Smith, E. Interplanetary magnetic field draping about fast coronal mass ejecta in the outer heliosphere. *J. Geophys. Res.* **1988**, *93*, 2519–2526. [CrossRef]

44. McComas, D.; Gosling, J.; Bame, S.; Smith, E.; Cane, H. A test of magnetic field draping induced B z perturbations ahead of fast coronal mass ejecta. *J. Geophys. Res.* **1989**, *94*, 1465–1471. [CrossRef]

45. Kataoka, R.; Shiota, D.; Kilpua, E.; Keika, K. Pileup accident hypothesis of magnetic storm on 17 March 2015. *Geophys. Res. Lett.* **2015**, *42*, 5155–5161. [CrossRef]

46. Choraghe, K.; Shaikh, Z.; Raghav, A.; Ghag, K.; Dhamane, O. Intense (SYM-H ≤ -100 nT) Geomagnetic Storms Induced by Planar Magnetic Structures in Co-rotating Interaction Regions. *Adv. Space Res.* 2023, *in press.*

47. Bergin, A.; Chapman, S.C.; Watkins, N.W.; Moloney, N.R.; Gjerloev, J.W. Extreme Event Statistics in Dst, SYM-H, and SMR Geomagnetic Indices. *Space Weather* **2023**, *21*, e2022SW003304. [CrossRef]

48. Yermolaev, Y.I.; Lodkina, I.; Nikolaeva, N.; Yermolaev, M.Y. Influence of the interplanetary driver type on the durations of the main and recovery phases of magnetic storms. *J. Geophys. Res. Space Phys.* **2014**, *119*, 8126–8136. [CrossRef]

49. Shaikh, Z.I.; Raghav, A.N. Evolution of Earth's magnetosheath as a planar magnetic structure. *Mon. Not. R. Astron. Soc.* **2022**, *511*, 4963–4970. [CrossRef]

50. Kamide, Y.; McPherron, R.; Gonzalez, W.; Hamilton, D.; Hudson, H.; Joselyn, J.; Kahler, S.; Lyons, L.; Lundstedt, H.; Szuszczewicz, E. Magnetic storms: Current understanding and outstanding questions. *Magn. Storms* **1997**, *98*, 1–19.

51. Aguado, J.; Cid, C.; Saiz, E.; Cerrato, Y. Hyperbolic decay of the Dst index during the recovery phase of intense geomagnetic storms. *J. Geophys. Res.* **2010**, *115*, 7220.

52. O'Brien, T.; McPherron, R. Evidence against an independent solar wind density driver of the terrestrial ring current. *Geophys. Res. Lett.* **2000**, *27*, 3797–3799.

53. Borovsky, J.E.; Thomsen, M.F.; Elphic, R.C. The driving of the plasma sheet by the solar wind. *J. Geophys. Res.* **1998**, *103*, 17617–17639.

54. Jordanova, V.; Kistler, L.; Thomsen, M.; Mouikis, C. Effects of plasma sheet variability on the fast initial ring current decay. *Geophys. Res. Lett.* **2003**, *30*, 6. [CrossRef]

55. Liemohn, M.W.; Kozyra, J.; Thomsen, M.; Roeder, J.; Lu, G.; Borovsky, J.; Cayton, T. Dominant role of the asymmetric ring current in producing the stormtime Dst. *J. Geophys. Res.* **2001**, *106*, 10883–10904. [CrossRef]

56. Fenrich, F.; Luhmann, J. Geomagnetic response to magnetic clouds of different polarity. *Geophys. Res. Lett.* **1998**, *25*, 2999–3002. [CrossRef]

57. Wang, C.; Chao, J.; Lin, C.H. Influence of the solar wind dynamic pressure on the decay and injection of the ring current. *J. Geophys. Res.* **2003**, *108*.

58. Huttunen, K.; Koskinen, H. Importance of post-shock streams and sheath region as drivers of intense magnetospheric storms and high-latitude activity. In *Annales Geophysicae*; Copernicus Publications: Göttingen, Germany, 2004; Volume 22, pp. 1729–1738.

59. Guo, J.; Feng, X.; Emery, B.A.; Zhang, J.; Xiang, C.; Shen, F.; Song, W. Energy transfer during intense geomagnetic storms driven by interplanetary coronal mass ejections and their sheath regions. *J. Geophys. Res. Space Phys.* **2011**, *116*, A5. [CrossRef]

60. Yermolaev, Y.I.; Nikolaeva, N.; Lodkina, I.; Yermolaev, M.Y. Geoeffectiveness and efficiency of CIR, sheath, and ICME in generation of magnetic storms. *J. Geophys. Res. Space Phys.* **2012**, *117*, A9. [CrossRef]